Investigation of the Solution Conformation of Cytochrome *c*-551 from *Pseudomonas stutzeri*†

Mengli Cai,‡ Eric G. Bradford,§ and Russell Timkovich*,‡

Department of Chemistry, University of Alabama, Tuscaloosa, Alabama 35487-0336, and Boeing Computer Services, 1801 University Boulevard, Birmingham, Alabama 35294

Received March 31, 1992; Revised Manuscript Received June 24, 1992

ABSTRACT: ^{1}H NMR spectroscopy and solution structure computations have been used to examine ferrocytochrome *c*-551 from *Pseudomonas stutzeri* (ATCC 17588). Resonance assignments are proposed for all main-chain and most side-chain protons. Distance constraints were determined on the basis of nuclear Overhauser enhancements between pairs of protons. Dihedral angle constraints were determined from estimates of scaler coupling constants. Twenty-four structures were calculated by distance geometry and refined by energy minimization and simulated annealing on the basis of 1033 interproton distance and 57 torsion angle constraints. Both the main-chain and side-chain atoms are well defined except for a loop region around residues 34–40, the first two residues at the N-terminus and the last two at the C-terminus, and some side chains located on the molecular surface. The average root mean squared deviation in position for equivalent atoms between the 24 individual structures and the mean structure obtained by averaging their coordinates is 0.54 ± 0.08 Å for the main-chain atoms and 0.97 ± 0.09 Å for all non-hydrogen atoms of residues 3–80 plus the heme group. These structures were compared to the X-ray crystallographic structure of an analogous protein, cytochrome *c*-551 from *Pseudomonas aeruginosa* [Matsuura, Takano, & Dickerson (1982) *J. Mol. Biol. 156*, 389–409). The main-chain folding patterns are very consistent, but there are some differences. The largest difference is in a surface loop segment from residues 34 to 40.

Cytochromes *c*-551 are electron transport proteins found in prokaryotes, where they perform the same function as cytochrome *c* in eukaryotes. With ca. 82 amino acids they are simplified versions that express all the key characteristics of *c*-type cytochromes. Comparisons of structure and function have been reviewed (Kamen & Horio, 1970; Dickerson & Timkovich, 1975; Meyer & Kamen, 1982). Cytochromes *c*-551 comprise a family with sequence homologies. Several amino acid sequences are known (Ambler, 1982) and are readily aligned, showing regions of strict conservation, regions of change that can be interpreted as neutral substitutions (i.e., conservation of size and approximate hydrophobicity), and regions with some major changes such as a Pro/Gly or Arg/Ser switch. Any pair of proteins differ by approximately 25–35% of the sequence. A comparison of structures within the family thus affords an opportunity to explore sequence–structure–function interrelations with proteins that have passed through natural selection processes. The archetypical member of the family is cytochrome *c*-551 from *Pseudomonas aeruginosa* (PA[1] *c*-551). It is currently the only member of the family for which a detailed crystal structure is known (Dickerson et al., 1976; Almassy & Dickerson, 1978; Matsuura et al., 1982). It has been studied in depth by one-dimensional NMR techniques and recently has been well characterized in terms of proton (Chau et al., 1990; Detlefsen et al., 1990; Cai & Timkovich, 1991), nitrogen (Timkovich, 1990), and carbon (Timkovich, 1991) assignments by two-dimensional spectroscopy. Recently, global folding conformations of main-chain atoms were computed on the basis of NMR constraints (Detlefsen et al., 1991). Because of size, *c*-551 is a suitable system for application of 2D NMR solution structure techniques to explore structure differences within the family. The prototype crystal structure provides the opportunity for comparison of solution and solid-state conformations for homologous versions of *c*-551.

Cytochrome *c*-551 from *Pseudomonas stutzeri* (PS *c*-551) differs from PA *c*-551 at 26 positions (33%) as shown in Figure 1 (Ambler, 1963a,b; Ambler & Wynn, 1973). Some of the substitutions are neutral, such as Phe/Tyr interchanges, while others are potentially radical, such as Gly 11 (PA) to Pro 11 (PS) or the Arg/His change at 47. This report will present extensive assignments for the protons of PS *c*-551 and the results of distance geometry, energy minimization, simulated annealing, and restrained molecular dynamics calculations on the solution structure.

MATERIALS AND METHODS

Cytochrome *c*-551 from *Ps. stutzeri* (ATCC 17588) (PS *c*-551) was purified by adaptation of the procedure of Ambler and Wynn (1973). Cells were cultured as described in Robinson et al. (1979) on a standard medium (Parr et al., 1976) at pH 7 without copper sulfate. The purification included ammonium sulfate fractionation, batch treatment with DEAE-cellulose, chromatography on (carboxymethyl)cellulose in the pH range 3.9–4.6, and chromatography on DEAE-cellulose at pH 9.1. Complete details may be found in Cai (1991). As originally described by Ambler and Wynn (1973), two isozymes were isolated, with the major one containing pyroglutamic acid as the N-terminal residue, and the minor one,

† Financial support was provided in part by NIH Grant GM43292. This work was completed in partial fulfillment of the Ph.D. degree requirements of M.C.

* To whom correspondence should be addressed.

‡ University of Alabama.

§ Boeing Computer Services.

[1] Abbreviations: PA, *Pseudomonas aeruginosa*; PS, *Pseudomonas stutzeri*; 2D, two dimensional; DG, distance geometry; DQF-COSY, double-quantum-filtered correlation spectroscopy; E-COSY, enhanced correlation spectroscopy; EM, energy minimization; NOESY, nuclear Overhauser enhancement correlation spectroscopy; HOHAHA, homonuclear Hartmann–Hahn spectroscopy; NOE, nuclear Overhauser enhancement; RMD, restrained molecular dynamics; rmsd, root mean squared deviation; SA, simulated annealing.

0006-2960/92/0431-8603$03.00/0

```
Glu - Asp - Pro - Glu - Val - Leu - Phe - Lys - Asn - Lys - 10
Gln       Gly       Ala                             Ser

Gly - Cys - Val - Ala - Cys - His - Ala - Ile - Asp - Thr - 20
Pro       Ala                             Ser       Ala

Lys - Met - Val - Gly - Pro - Ala - Tyr - Lys - Asp - Val - 30
      Leu                                       Phe   Glu

Ala - Ala - Lys - Phe - Ala - Gly - Gln - Ala - Gly - Ala - 40

Glu - Ala - Glu - Leu - Ala - Gln - Arg - Ile - Lys - Asn - 50
Ala   Asp   Leu             Gly   His

Gly - Ser - Gln - Gly - Val - Trp - Gly - Pro - Ile - Pro - 60

Met - Pro - Pro - Asn - Ala - Val - Ser - Asp - Asp - Glu - 70
                        Pro       Thr   Glu   Glu

Ala - Gln - Thr - Leu - Gly - Lys - Typ - Val - Leu - Ser - 80
      Lys   Ile   Glu         Ile

Gln-Lys
```

FIGURE 1: Sequence comparison of cytochromes *c*-551 from *Ps. aeruginosa* (top line) and *Ps. stutzeri* (bottom line), showing the amino acid differences.

free glutamine. NMR confirmed the presence of pyroglutamic acid through the observation of a single, slowly exchanging amide proton at the first residue. All results to be described apply only to the pyroglutamic-containing isozyme. The modified purification procedure yielded protein with an increased purity ratio of 1.5, while the original procedure gave 1.2 (Ambler & Wynn, 1973).

Sample preparation and spectroscopic details for DQF-COSY, HOHAHA, and NOESY spectra have been described (Chau et al., 1990).

Distance constraints based upon NOESY cross-peak intensities were determined according to the methods of Williamson et al. (1985) and Dyson et al. (1990). NOESY spectra were recorded with mixing times of 50, 75, 100, 125, and 150 ms. Well-resolved NOESY cross peaks were examined and the volume integrals or peak heights were plotted versus mixing times. These buildup curves were linear up to 100 ms. Therefore, intensities in spectra with mixing times of 100 ms were used to estimate distance limits. For proton distances involving only main-chain protons, the upper distance boundaries were classified as 2.5, 3.0, 3.5, and 5 Å, corresponding to strong, medium, weak, and very weak NOE's, respectively. Assuming higher flexibility for the side chains, the upper boundaries were classified as 3.0, 4.0, and 5.0 Å, corresponding to strong, medium, and weak NOE's. Cross peaks involving only amide protons have characteristically different fine structures as described by Williamson et al. (1985) and so different boundaries were used. The upper boundaries were 3.0 and 4.0 Å for strong and weak NOE's, respectively. The heme group is buried in the protein and was considered relatively rigid, so its protons were treated in the same way as main-chain protons. For NOE's involving methyl groups, the upper boundaries were corrected for center averaging and an additional 0.5 Å was added to account for the higher intensity of the resonance (Clore et al., 1987; Wagner et al., 1987; Driscoll et al., 1989). In all cases, the lower boundary was set to 2.0 Å as approximately the sum of van der Waals radii. Pseudostructures were used for phenylalanine and tyrosine rings, and pseudoatoms were used for nonstereospecifically assigned methylene protons, as described by Wüthrich et al. (1983).

A total of 1033 interproton distance constraints were obtained from NOE's, which included 209 intraresidue, 303 sequential (for residues i and j, $j - i = 1$), 155 medium-range ($j - i < 5$), and 254 long-range ($j - i > 5$) NOE's and 112 NOE's from the heme group to peptide protons. These distance constraints were obtained in two stages. In the first stage, only well-resolved and unambiguously assigned NOE's were converted into distance constraints. A total of 593 distance constraints were identified, including 209 intraresidue and 326 interresidue NOE's and 58 NOE's from the heme group to peptide protons. These constraints along with 57 dihedral angle constraints, discussed in the following paragraph, were used to compute a preliminary structure for PS *c*-551. Details of this are described in the Structure Computation subsection. With the preliminary structure available, additional NOE's could now be assigned with confidence in the second stage. NOE's assigned from overlapping cross peaks, where the intensity could be ambiguous because of the overlap, were assigned to the very weak class and the upper boundary was set to 5 Å. An example of the second-stage process will illustrate the approach taken. The heme 5 meso proton showed a weak but definite NOE to a proton at 2.58 ppm. At this chemical shift there are a number of degenerate resonances that had been unambiguously assigned by scalar correlation data, including β protons of Tyr 34, Asn 64, and Ser 52. In the preliminary structure, these were respectively 16.5, 4.9, and 9.7 Å from the heme meso proton. So although we could not differentiate on the basis of chemical shifts, the preliminary structure allowed the NOE to be assigned to Asn 64 and then added to the list of distance constraints. It would have taken a gross rearrangement of global folding, including disruption of obvious secondary structure elements (α helices) to place the other candidates close to the meso proton.

Dihedral angle constraints were estimated on the basis of scalar coupling as described by Driscoll et al. (1989). By estimating the width of the cross peak from a main-chain amide proton to an α proton in HOHAHA spectra, and by the peak-to-peak separation in high digital resolution DQF-COSY spectra, 17 coupling constants were identified that were larger than 8 Hz and 33 that were smaller than 5.5 Hz. Corresponding main-chain ϕ torsional angles were constrained to be in the range $-80°$ to $-160°$ for the former and $-40°$ to $-90°$ for the latter. All seven prolines were identified as being in the trans conformation and were constrained to an ω anlge of 175–185°. No constraints were applied to glycine residues.

Stereospecific assignments were made for 15 β methylene proton sets on the basis of the criteria of Wagner et al. (1987), by examination of DQF-COSY, HOHAHA, and NOESY spectra. From these assignments, 12 χ angles were constrained to $-60 \pm 60°$, and three were constrained to $180 \pm 60°$. Three valine residues were identified as belonging to the g^+ rotamer (χ, $-60 \pm 60°$) and one to the g^- rotamer class (χ, $60 \pm 60°$), according to the classification of Zuiderweg et al. (1985).

Structure Computations. The crystal structure coordinates (Matsuura et al., 1982) of PA *c*-551 were obtained from the Brookhaven Protein Data Bank. The graphics and molecular modeling software package SYBYL (Tripos Associates, St. Louis, MO) was used for display and initial structure analysis. SYBYL was used to add hydrogen atoms to the heavy atoms in standard geometries and to change residue side chains to superimpose the PS *c*-551 sequence on the global fold of PA *c*-551. In this process, SYBYL uses as many of the side-chain coordinates of the original residue as possible, while for unique atoms it adds then in a standard relative geometry. This standard geometry does not account for interresidue contacts, so it did introduce some steric conflicts. The PS structure after side-chain replacement was energy-minimized by MAXMIN2 with steepest descent approach (Levitt, 1982). The total conformation change was very small, with an rmsd of 0.14 Å over all non-hydrogen atoms, but bad van der Waals conflicts involving the edited side chains were removed.

This structure was subjected to refinement with NMR constraints by a combination of restrained molecular dynamics and energy minimization using the software package NMR4 running on a Cray XMP computer. NMR4 is a version of AMBER (Weiner & Kollman, 1981) that incorporates distance and dihedral constraints based upon NMR into the structure refinement as described by Gippert et al. (1990). In general the AMBER all-atom force field (Weiner et al., 1986) was used, while for bonds involving iron, force constants were taken from CHARMM (Brooks et al., 1983). The potential function associated with the NMR constraints was zero for distances and torsion angles between the upper and lower bounds, rose parabolically as a penalty function when the bounds were exceeded, and rose linearly if the bounds were exceeded by some maximum amount, user-selectable and typically 0.5–1.0 Å. The force constant for the penalty was typically 32 kcal for both distances and angles. Different calculations indicated that the magnitude of the force constant was not critical because, as will be discussed, there were only very minor constraint violations in the refined structure and the total contribution of the NMR penalty function was always small.

The protocol to produce the preliminary structure used the first-stage set of constraints described earlier and the following conditions. For the dynamics a nonbonded interaction cutoff of 9 Å was selected and the equations of motion were integrated in steps of 1 fs. The system was kept at the initial temperature of 0 K for 1 ps and then increased to 1000 K by a temperature-regulated algorithm (Berendsen et al., 1984) with a relaxation time of 0.2 ps. This was followed by 4 ps of equilibration at 1000 K with a relaxation time of 0.05 ps. Then the temperature was slowly cooled to 0 K during a 6-ps period with a relaxation time of 0.05 ps. The system was then equilibrated again for 1 ps at 0 K. A final 1000 cycles of conjugated energy minimization without NMR constraints was carried out in case the NMR constraints had introduced any slight distortions in standard geometries. Subsequent analysis indicated that the constraints had not done so.

This protocol produced a single structure that will be designated RMD (for restrained molecular dynamics). It is of low internal energy and the dynamics with annealing should ensure that the conformation is not a local energy minimum far from the true global minimum. It is consistent with an unambiguous but limited set of NMR constraints. It could be criticized, however, on the following grounds. By starting with main-chain crystal coordinates from PA, the RMD structure was produced without a wide initial search of conformational space. This raises the question of how well the NMR data actually determine the conformation. The question was addressed by use of the distance geometry algorithm.

Starting structures were generated by a distance geometry/structure refinement program X-PLOR/dg (Kuszewski et al., 1992). X-PLOR/dg translates covalent geometry from X-PLOR parameter files into interatomic distance constraints, adds experimentally derived constraints, and creates a matrix of upper and lower bounds on the distances between all pairs of atoms in the system. It optionally uses a distance geometry protocol, partial metrization, which can improve the conformational energy of embedded structures and the sampling of conformational space. However, metrization may be somewhat problematic when used for full structure embedding without prior substructure embedding (Brünger, personal communication), which was not present in the experimental version of X-PLOR/dg available to us at the time. For PS c-551, a total of 40 DG structures were generated, 20 with random partial metrization and 20 with no metrization. Each

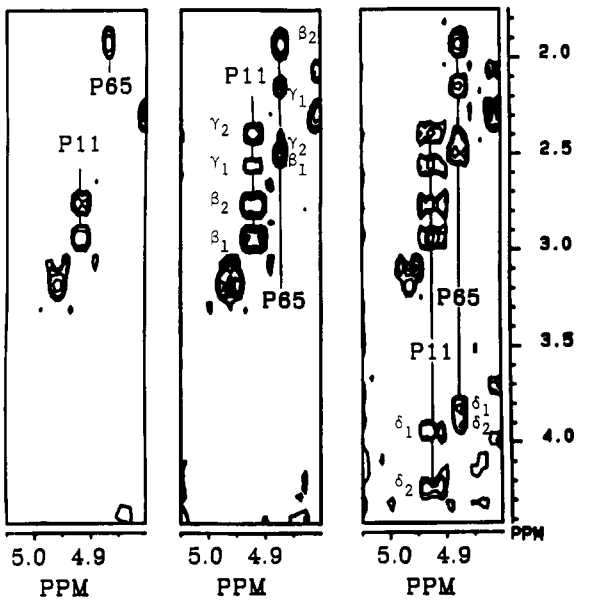

FIGURE 2: HOHAHA spectra of different spin lock times showing the progressive assignments of Pro 11, Pro 58, Pro 60, and Pro 65 of PS c-551. All spectra were recorded at pH 4.75 and 47 °C and the following spin lock times: (left) 5 ms, (center) 20 ms, and (right) 75 ms. The vertical lines mark the residue spin systems. Cross peaks appear in the left panel for direct α–β coupling, then in the center panel as relayed coupling to γ, and finally in the right panel as relayed coupling to δ protons.

structure was generated with a different random seed number. To reduce the computer memory requirements, each methyl group was replaced with a single pseudoatom (Wüthrich et al., 1983) during the distance geometry and structure regularization calculations, while all atoms were used during simulated annealing calculations. When the methyl pseudoatom was used, upper boundaries relating to methyls were increased by 0.36 Å.

The embedded DG structures were regularized by a multistage minimization protocol with a variable target function developed by Kuszewski et al. (1992). Regularized structures were further refined by a simulated annealing method (Nilges et al., 1988; Brünger & Karplus, 1991). Nonbonded terms were replaced by a simple van der Waals repulsion term. The initial force constants were set to 50, 200, and 500 kcal/(mol rad^2) for improper, angle, and torsion angle constraint terms, respectively, and 1000, 0.002, and 50 kcal/(mol Å^2) for bond, repulsion, and NOE constraints, respectively. For the dynamics, the Verlet integration method was used and the equations of motion were integrated in steps of 1 fs. After a 300-step Powell energy minimization, initial velocities were randomly assigned at 1000 K according to a Maxwell distribution. After 2 ps, the van der Waals repulsion constant was increased by multiplying its value every 75 fs until it reached 4.0 kcal/(mol Å^2). The force constants for angle and improper torsion terms were set to 500 kcal/(mol rad^2), and the system was integrated for another 4 ps at 1000 K. In the cooling stage, van der Waals constants were multiplied by 0.8 and the velocities were rescaled to 300 K by reducing the temperature by 25 K every 50 fs. Structures were finally subjected to 500 cycles of restrained energy minimization.

For the 20 structures generated with random partial metrization, eight structures were identified as having wrong chirality compared to the RMD and other 12 structures. The 12 plus RMD all had the same global fold. Of the 12, 10 were in excellent agreement with the experimental constraints with no distance violations greater than 0.4 Å and no torsion angle

Table I: Proton Resonance Assignments for PS *c*-551

residue[a]	chemical shift[b] (ppm) NH	C_α	C_β	C_γ	C_δ	C_ϵ	other
X_1[c]	8.30	4.35	2.55, 2.03	2.45			
D2	7.79	3.80	1.28				
G3	8.72	3.26, 3.11					
E4	7.25	2.85	1.89	2.20, 2.30			
A5	7.49	3.99	1.45				
L6	7.75	4.13	1.90, 1.35*	1.72	0.93, 0.93		
F7	8.21	4.25	2.95				C2 (C6), 7.18; C3 (C5), 6.94; C4, 7.02
K8	7.46	3.77	1.82	1.42	2.08	2.98	
S9	7.75	4.62	4.12, 3.97				
K10	7.66	5.17	2.72*, 2.27	2.05	1.44, 1.63	2.95	
P11		4.93	2.92, 2.75	2.53, 2.38	3.92, 4.22		
C12	8.23	4.95	3.19, 3.08*				
A13	8.15	4.23	1.03				
A14	7.84	4.20	1.76				
C15	6.76	4.33	1.82, 1.00*				
H16	7.08	3.78	0.63, 0.00*				C2, 0.68; C5, 0.72; Nπ, 8.75
S17	7.28	4.26	3.52, 3.63				
I18	8.28	3.26	1.68	1.43, 0.88			γ-CH_3, 0.69; δ-CH_3, 0.75
D19	7.98	4.57	2.67				
A20	7.22	4.43	1.08				
K21	8.32	3.59	1.62	1.00, 1.08	1.51	2.83	
L22	7.31	4.33	1.12, 0.79*	0.42, 1.07	1.04		
V23	6.96	3.98	1.83	1.59, 1.14*			
G24	6.61	0.08, 3.67					
P25		3.51	0.82, 0.48	0.03, 0.08	2.82, 2.05		
A26	8.07	3.86	0.75				
F27	7.73	4.20	2.52*, 2.75				C2 (C6), 6.01; C3 (C5), 5.13; C4, 5.48
K28	8.86	4.00	1.73	1.42, 1.26	1.56	2.83	
E29	6.78	4.27	2.15	2.37			
V30	7.62	4.12	2.32	1.67, 0.84*			
A31	8.35	4.00	1.55				
A32	7.38	4.18	1.55				
K33	7.85	4.01	2.05*, 1.90	0.38, 1.00	1.20	2.50	
Y34	7.42	4.60	2.58*, 3.42				C2 (C6), 7.53; C3 (C5), 7.30
A35	7.52	4.24	1.54				
G36	8.74	3.91, 4.15					
Q37	7.90	4.53	2.26	2.42			NH_2, 7.68, 6.79
D38	8.87	4.54	2.68				
G39	8.82	4.07, 4.07					
A40	7.63	4.01	1.62				
A41	8.74	3.83	1.38				
D42	7.55	4.31	2.59				
L43	7.44	3.86	1.42, 1.70	1.58	0.85, 0.78		
L44	8.49	3.75	1.42, 1.97	1.72	0.89, 0.77		
A45	8.43	3.87	1.41				
G46	7.49	3.71, 3.91					
H47	7.26	4.27	2.15, 2.95*				C2, 8.62; C5, 7.09
I48	8.34	1.49	1.63	1.65, 1.12			γ-CH_3, 0.72; δ-CH_3, 1.31
K49	7.33	3.80	1.65	1.27	1.47	3.02, 3.10	
N50	7.98	4.68	2.81, 2.70				$NH_{2,\ 6.95,\ 7.29}$
G51	7.12	3.55, 2.05					
S52	7.02	3.95	2.58				
Q53	7.62	4.29	1.83, 1.92	2.05, 2.25			NH_2, 6.66, 7.31
Q54	8.28	4.21, 3.92					
V55	10.48	3.83	2.50	1.01*, 0.75			
W56	10.63	4.65	3.70, 3.80				C2, 7.80; C4, 7.97; C5, 7.26, C6, 7.08; C7, 7.66; N_{indole}, 12.73
G57	8.08	4.20, 4.60					
P58		4.80	2.28	2.05, 2.26	3.95, 3.69		
I59	7.48	4.72	2.20	1.82, 1.51			γ-CH_3, 1.42; δ-CH_3, 1.12
P60	4.75	2.00, 1.51	2.15, 2.00	3.90, 4.10			
M61	8.48	3.65	–0.88*, –2.69	–0.52, –3.65			S-CH_3, –2.907
P62		4.22	1.52, 1.98	1.79, 1.93	3.62, 3.67		
P63		3.33	1.54, 2.07	1.75, 1.62	3.22, 3.29		
N64	7.03	5.18	2.58*, 1.98				NH_2, 7.02, 3.20
P65		4.87	1.92, 2.49	2.39, 2.15	3.80, 3.91		
V66	8.02	5.06	2.49	0.61*, 0.77			
T67	8.78	4.51	4.80	1.31			
E68	9.12	3.90	2.05	2.38			
E69	8.41	4.07	2.12, 1.95	2.33			
E70	7.83	4.55	2.35, 2.52	2.75, 2.93			
A71	8.61	4.00	1.56				
K72	7.83	4.02	2.05, 1.87	1.72, 1.47	1.65, 1.32	3.00	
I73	8.02	3.81	1.88	1.17, 1.83			γ-CH_3, 0.84; δ-CH_3, 0.83
L74	8.58	4.27	1.68, 2.49*	1.92	1.26, 1.26		
A75	8.67	4.00	1.70				
E76	8.44	4.03	2.23, 2.04	2.46, 2.68			
W77	8.38	4.33	3.36, 3.43*				C2, 7.40; C4, 7.42; C5, 6.20; C6, 6.25; C7, 7.21; N_{indole}, 10.21
I78	8.96	2.63	1.90	1.76, –0.66			γ-CH_3, 0.63; δ-CH_3, 0.92
L79	7.98	3.90	1.94*, 1.64	1.89	0.96, 1.28		
S80	7.42	4.48	3.99, 4.09				
Q81	7.37	3.95	1.68, 1.82	2.10, 1.28			NH_2, 5.54, 5.16
K82	7.36	4.05	1.75, 1.65	1.47, 1.35	1.70, 1.63	2.89	

Table I (Continued)

type of heme proton	no.	chemical shift (ppm)	type of heme proton	no.	chemical shift (ppm)	type of heme proton	no.	chemical shift (ppm)	type of heme proton	no.	chemical shift (ppm)	type of heme proton	no.	chemical shift (ppm)
meso proton	5	9.89	ring methyl	2^1	3.72	bridge methine	3^1	6.01	propionate 13	1a	4.28	propionate 17	1a	4.08
	10	9.32		7^1	3.75		8^1	6.25		1b	4.55		1b	4.73
	15	9.37		12^1	3.30	bridge methyl	3^2	1.96		2a	3.35		2a	2.71
	20	9.21		18^1	3.42		8^1	2.52		2b	2.65		2b	3.55

[a] Amino acids are listed with the one-letter code. [b] Chemical shifts (ppm) are referenced to dioxane at 3.74 ppm, and the reported shifts were obtained from the sample recorded at pH 4.75 and 47 °C. The stereospecific assignments are denoted as follows. For the C^{β} methylene protons, the asterisk indicates the $H^{\beta 2}$ proton (Wagner et al., 1987); for valine methyl groups, the asterisk indicates $C^{\gamma 1}$ (Zuiderweg et al., 1985). Methylene protons of residues 6, 10, 12, 15, 16, 22, 27, 34, 47, 64, 74, and 79 are classified as t^2g^3 rotamers, and the methylene protons of residues 33, 61, and 77 are classified as $g^{2\pm}3$ rotamers (Wagner et al., 1987). Val 23, Val 30, and Val 55 are classified as g^+ rotamers, and Val 66 is classified as a g^- rotamer (Zuiderweg et al., 1985). [c] The N-terminal residue in PS *c*-551 is pyroglutamic acid.

constraints greater than 2°. One of the 10 had a positive ϕ angle of 46° for residue 26 and had a higher energy than the other nine. This structure was considered as a possible local minimum conformation and was excluded from the other nine. For the 20 structures generated with no metrization, three had wrong chirality and two had excessive constraint violations. The remaining 15 had no constraints violations greater than 0.4 Å and 2°. Two of the 15 had energy and constraint violations noticeably higher than the remaining thirteen. The 24 structures out of the total 40 that best satisfied the experimental data were selected for further analysis.

A mean structure, designated ⟨SA⟩, was obtained by best-fitting the 24 SA structures to each other and averaging their coordinates (Driscoll et al., 1989). Irregularities due to the simple averaging process were corrected by 1000 cycles of restrained energy minimization to yield the minimized mean structure, ⟨SA⟩r.

Side-chain χ angle constraints from the stereospecifically assigned methylene protons were not initially used in the SA or ⟨SA⟩r refinements. They were added to the ⟨SA⟩r refinement process in the later stages. However, the SA structures all satisfied the range limits for these constraints, and the additional constraints therefore had minimal impact.

As mentioned previously, structures were refined with a simple van der Waals repulsion term for nonbonded atoms (Nigles et al., 1988) to produce the SA and ⟨SA⟩r structures. Additional calculations were performed to investigate the consequences of more elaborate force fields for nonbonded atoms. ⟨SA⟩r was further refined in 500 cycles with the normal X-PLOR force fields that include electrostatic terms to produce a structure termed ⟨SA⟩r,el. An additional 500 cycles of refinement was performed with the addition of the X-PLOR hydrogen bond force field to produce a structure termed ⟨SA⟩r,el,hb. The hydrogen bond terms act to regularize the angle of potential hydrogen bonds.

RESULTS

Assignments. Proton assignments were completed in stages. Side-chain aromatic and heme protons were assigned on the basis of distinctive patterns in DQF-COSY and NOESY spectra. Select resonances have unusual chemical shifts because of the heme ring current. These and the aromatic residues are easily assigned, especially because of analogy to PA *c*-551. These resonances became valuable landmarks for the sequential assignment process through NOE's to main-chain and aliphatic side-chain protons. Side-chain spin system types were initially categorized through α, β, and some γ cross peaks in the fingerprint region of HOHAHA spectra recorded in ^1H_2O. It was especially helpful to record spectra at different temperatures and pH values. The amide protons are sensitive to these and shift around. The cross peaks of the associated side-chain protons in the fingerprint region move with the amide as a unit and this helps to overcome accidental degeneracy at a single set of conditions. Sequential assignments were then made by means of interresidue NOE's among amide, α, and β protons. Not all of the protons of a side chain spin system necessarily appear in the fingerprint region of HOHAHA spectra even at long spin lock times. Side-chain assignments were completed as fully as possible by interpretation of the aliphatic region of HOHAHA and DQF-COSY spectra recorded in ^2H_2O. It was especially informative to record HOHAHA spectra at increasing spin lock times and to follow the appearance of additional protons of the spin system. The complete side chains of proline residues, which do not appear in the fingerprint region of scalar correlation spectra, were assigned in this manner. Figure 2 illustrates

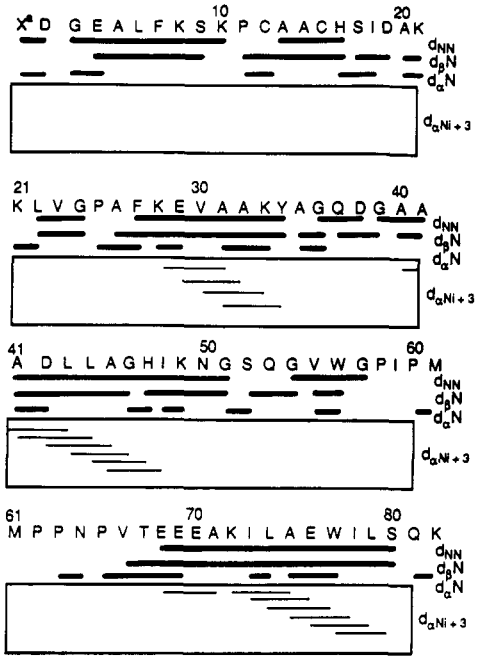

FIGURE 3: Summary of sequential connectivities for PS *c*-551. A bar indicates a NOESY cross peak was observed between the two residues. The letter X was chosen arbitrarily as the one-letter code for pyroglutamic acid.

this for four proline residues. Looking in the chemical shift region of the α proton, one sees cross peaks to β protons at short spin lock times, then to γ protons at longer times, and finally to δ protons. In favorable cases where there is sufficient resolution, one can confirm these assignments by looking in the δ regions and progressively observing the appearance of γ, β, and α resonances. Finally, DQF-COSY spectra are checked for the presence of cross peaks for direct scalar coupled protons. Further extensive details, documentation, and labeled spectra for the assignments have been given in Cai (1991). Resonance assignments are given in Table I, and Figure 3 summarizes sequential connectivities.

Structure Statistics. Structure statistics for the best 24 SA structures are given in Table II. All 24 SA structures and the refined mean structure ⟨SA⟩r display only small deviations from idealized covalent residue geometry and have good nonbonded contacts as indicated by small values for the repulsive force and a negative value for van der Waals energies.

The overall fold of the protein is displayed in Figure 4 by a ribbon diagram for ⟨SA⟩r. Superposition of the main-chain atoms for the 24 SA structures is shown in Figure 5. The conformation of all main-chain atoms is well conserved except for the first two N-terminal residues, the last two C-terminal residues, and a loop region from residues 34 to 40. This is reflected by the small average rmsd of 0.7 Å of each SA structure to ⟨SA⟩. The distribution of rmsd values as a function of residue number is shown in Figure 6. Deviations of the ϕ and ψ angles are shown in Figure 7. All non-glycine residues except for Gln 53, whose ϕ angle was in the range of $-174 \pm 15°$, lie within the sterically favorable region of a Ramachandran plot (Figure 8). Side-chain atoms are determined to the extent as shown in Figure 6. The average rmsd value for the 24 SA structures and ⟨SA⟩ was 1.12 Å for all heavy atoms. Specific side chains with large individual deviations are located on the molecular surface and have large accessible surface areas as shown in Figure 6. Most are highly charged residues such as lysines and glutamic acids.

The addition of a force field with electrostatic terms to produce ⟨SA⟩r,el and then with terms to regularize hydrogen-bond geometry to produce ⟨SA⟩r,el,hb had minimal impact on the ⟨SA⟩r structure. Hydrogen bonds in elements of secondary structure such as helices and turns were in general well-defined without the additional refinement. There were a few cases involving groups far apart in sequence but close in space where the additional refinement improved the geometry of hydrogen bonds. These will be discussed on a case by case basis.

Table II: Structures Statistic for PS *c*-551

	SA[a]	⟨SA⟩r
Distance Constraints		
av. no. of violations		
$0.1 \text{ Å} \le d < 0.2 \text{ Å}$	9.79	8
$0.2 \text{ Å} \le d < 0.3 \text{ Å}$	1.63	1
$0.3 \text{ Å} \le d < 0.4 \text{ Å}$	0.42	0
max violation (Å)	0.35	0.25
rmsd from upper bounds[b] (Å)		
intraresidue	0.024	0.030
sequential	0.029	0.040
short range	0.017	0.022
long range	0.014	0.014
Torsion Angle Constraints		
av no. of violations > 0.5 deg	1.13	1
max violation (deg)	1.7	0.7
Energies[c] (kcal/mol)		
F_{noe}	26 ± 6	18.5
F_{tor}	0.2 ± 0.1	0.08
F_{repel}	4.0 ± 1.0	2.4
E_{L-J}	-496 ± 11	−502
Rmsd from Idealized Geometry		
bonds (Å)	0.007	0.007
angles (deg)	2.2	2.2
impropers (deg)	0.6	0.6

	SA vs ⟨SA⟩	⟨SA⟩ vs ⟨SA⟩ r
Atomic Rmsd (Å)		
whole protein		
main chain	0.7 ± 0.1	0.47
all	1.1 ± 0.1	0.67
residues 3–80 plus heme group		
main chain	0.54 ± 0.08	0.26
all	0.97 ± 0.09	0.45

[a] SA represents the 24 individual structures refined by the simulated annealing method described in the text. ⟨SA⟩ is the mean structure obtained by simple averaging of the coordinates of the SA structures. ⟨SA⟩r is the refined structure obtained by energy minimization of ⟨SA⟩ as described in the text. [b] Root mean squared deviations in angstroms when the calculated final distance between protons in the structure after simulated annealing refinement exceeds the upper bounds of the NOE distance constraint, averaged over all constraints. Values are groups into intraresidue and interresidue classes as discussed in the text for the different types of constraints. [c] The force constants used for these calculations were 50 kcal/(mol Å^2) for NOE's, 500 kcal/(mol rad^2) for torsion angles, and 4 kcal/(mol Å^2) for repulsion terms. F_{noe}, F_{tor}, and F_{repel} are, respectively, the violation energies associated with NOE's, torsion angles, and the van der Waals repulsion energy with hard-sphere van der Waals radii set to 0.8 times the standard value used in the CHARMM empirical energy function (Brooks et al., 1983). E_{L-J} is the van der Waals energy recalculated with the same coordinates but using the X-PLOR energy function.

DISCUSSION

Global Folding in Solution. The solution structure of PS *c*-551 consists of four major α helices and one major polyproline-type helix connected by turns and loops. α-Helical regions are identified qualitatively by distinctive patterns of NOE's and quantitatively in the SA structures by their ϕ and ψ torsional angles (average values in PS *c*-551 helices are −66° and −39°, respectively). α Helices extend from Gly 3 to Lys 9, from Phe 27 to Lys 33, from Ala 40 to Lys 49, and from Glu 69 to Ile 79. A pronounced polyproline helix, identified with average ϕ and ψ values of −84° and 143°,

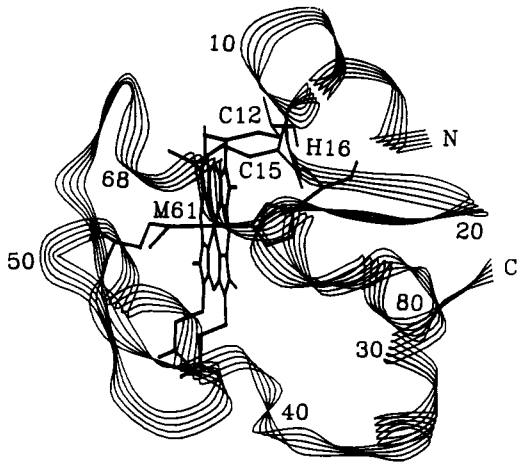

FIGURE 4: Ribbon diagram of the minimized mean structure showing the global folding of *Ps. stutzeri* ferrocytochrome *c*-551.

extends from Ile 59 to Gln 63. Another very short segment from residues 24 to 26, including Pro 25, has polyproline-type helix character with average ϕ and ψ values of –69° and 144°. Pro 25 is sequence conserved over many pseudomonad cytochromes. It appears to form a critical hydrogen bond from its carbonyl oxygen to the non-iron-bonded imidazole nitrogen of the heme ligand His 16, where it may help to orient the imidazole with respect to the heme plane.

Comparison to the Crystal Structure of PA c-551 (Matsuura et al., 1982). The solution computed structures of PS *c*-551 and the crystal structure of PA *c*-551 have a very similar fold. The average rmsd for all main-chain atoms between ⟨SA⟩r and the crystal structure is 1.23 Å from residues 3–80 plus the heme. This number includes some obvious differences imposed by amino acid substitutions between the proteins. Relative packing of side chains is different due to substitutions and this can lead to a constant shift of an element of secondary structure. Substitutions involving prolines are a main cause of differences. In computer docking experiments, if one superimposes only main-chain atoms for select small segments, then the rmsd becomes smaller. In the ensuing discussion, attention will be focused on areas of largest differences. Definitions of secondary structure elements in terms of ϕ and ψ angles have been taken from Crawford et al. (1973).

The N-Terminal Helix and Pro 11. Pro 11 occupies a peculiar position in the protein, since it is just prior to the first thioether covalent attachment of the heme to Cys 12. In the crystal structure of PA *c*-551, which has Gly 11, the N-terminal α helix extends roughly from residues 4 to 11, but at the end of this run the four residues 8–11 form a type I turn. Residues 12–15 form a 3_{10} helix segment that positions the two thioether attachment points, and a rotation at 15 positions His 16 to act as the fifth heme ligand. It seems that, without these anchor points, residues 4–16 could form a continuous single helix, so it is reasonable to ascribe the heme attachment as exerting a major influence on peptide conformation in this region. The switch from Gly 11 in PA to Pro 11 in PS cannot be called a structurally neutral mutation, because of the increased bulk and closed covalent structure of the side chain. In ⟨SA⟩r, the main-chain torsion angle of Pro 11 and Lys 10 has rotated more than 100° compared to PA to release bad van der Waals contacts. As a result, the type I turn was replaced with a distorted type III turn consisting of the sequence Lys 10, Pro 11, Cys 12, and Ala 13. Distortion and the short length of the preceding segment from residues 3 to 9 may also account for the failure to observe $d_{N(i+1)}$ NOE cross peaks above the noise level (Figure 3), although the other amide NOE's are typical of helical secondary structure. There are two side-chain size changes (PA Val 5 and Val 13 to PS Ala 5 and Ala 13) in this region, but this seems to have little impact on structure. Both residues are on the outside surface of the protein.

The secondary structure change around Pro 11 is reflected by chemical shift differences for the amide protons at positions 8 (0.5 ppm), 10 (1.29 ppm), and 13 (1.52 ppm). The differences are interpreted as due to changes in hydrogen bonding, as has been noted in other studies (e.g., Gao et al., 1989). In PA *c*-551, the amide protons of Lys 10, Gly 11, and Val 13 are hydrogen-bonded to the carbonyl oxygens of residues 6, 8, and 7, respectively, while in PS *c*-551 ⟨SA⟩r, the hydrogen bond between Lys 8 and Pro 11 is gone and the amide of Ala 13 is hydrogen-bonded to the carbonyl oxygen of Lys 10 instead of Phe 7. This 10–7 hydrogen bond pulls the carbonyl oxygen of Ala 10 near to its own amide proton (4.2 Å in PA, 2.9 in PS) and thus changes the environment and chemical shift of the amide.

Pro 65. The sequence from residues 65 to 67 is located at the end of the polyproline helix and before the C-terminal helix. Looking only at the sequence of residues, the substitution of Pro 65 in PS for Ala 65 in PA could potentially have extended the polyproline helix in PS. However, this was not the case and in PS the segment is still a short loop interconnecting the two helices. On the basis of the ϕ and ψ values it cannot be classified into any regular element of secondary structure. The substitution does lead to a big change in the size of the side chain. Model building indicated that without some change in torsion angles there would have been bad van der Waals contacts.

Loop 35–40. The largest change between the crystal structure of PA and ⟨SA⟩r is in a surface loop region around residues 35–40. This loop occurs at the end of the 27–33 α helix and before the 40–49 helix and causes a major change in direction for the main-chain path. In this region of PS, there were NMR constraints for the ϕ angles of residues 35, 37, 38, and 40, and many intraresidue and sequential NOE's were identified. However, only two long-range NOE's were found, in spite of intensive efforts for these resonances both in the first stage before the RMD model structure was available and afterward in the second stage. The high rmsd values between SA structures is ascribed to this lack of long-range NOE's.

In the sequence from Tyr 34 to Ala 40 there are two turns. In ⟨SA⟩r they were a single left-handed helix turn at Gly 36 (ϕ = 49°, ψ = 17°) and a distorted type II turn from Gln 37 to Ala 40 with ϕ and ψ values of –42° and 144° at Asp 38 and 92° and –27° at Gly 39. However, other conformations were consistent with the experimental constraints and had low energies. From Tyr 34 to Gly 37, eight distorted type II turns and two distorted type I turns were also identified among the 24 SA structures. From Gln 37 to Ala 40, additional turns appeared among the 24 SA structures including three type III turns, five type I turns, seven left-handed helical type turns, and four turns that cannot be placed into an obvious turn category yet were within sterically allowed Ramachandran space.

In the crystal structure of PA *c*-551, there is a type I turn from residues 34 to 37 and a type II turn from residues 37 to 40. Although there are two side-chain substitutions in this region for PA versus PS, they are probably neutral changes, especially since the Asp 38 side chain is solvent-exposed.

Although the refined SA structures are not well defined for the loop, there are several pieces of NMR data that indicate there may be real differences between the crystal and solution conformations in this region. The data suggest that this change

FIGURE 5: Stereoview of the best-fit superposition of the 24 SA structures. The main-chain atoms (nitrogen, α-carbon, and carbonyl carbon) are shown with the heme and the side chains of heme ligands and the thioether bridges.

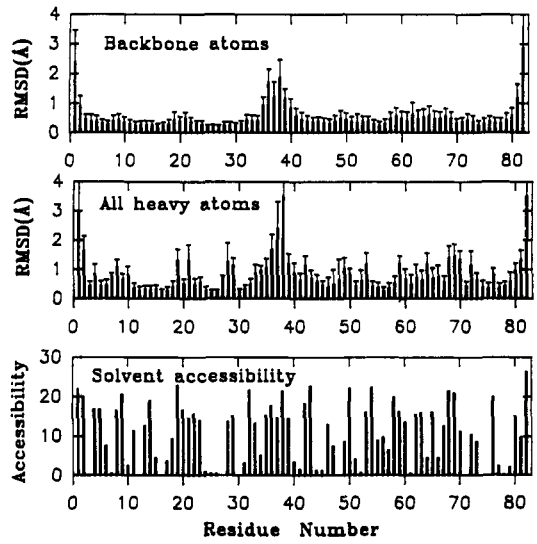

FIGURE 6: Atomic rmsd distribution of the individual SA structures about the mean structure, ⟨SA⟩, and the surface accessibility of residues in the minimized mean structure, ⟨SA⟩r. The filled bars represent the average values, and standard deviations are shown by the vertical error bars on the top.

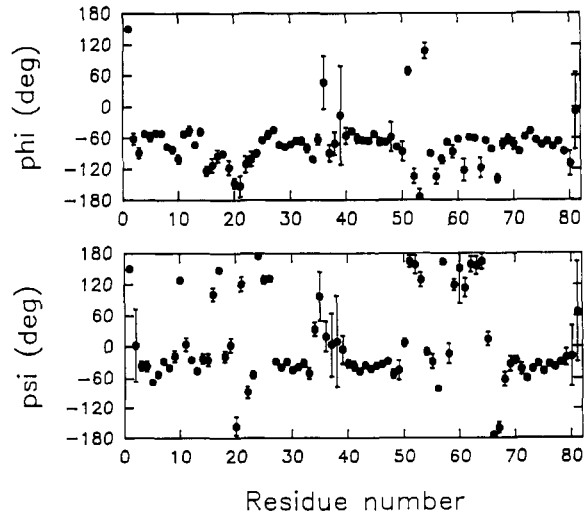

FIGURE 7: Angular rmsd distribution of the ϕ and ψ main-chain torsion angles of the individual SA structures. The filled circles represent the average values, and standard deviations are shown by the vertical error bars.

is not a difference between PA and PS but is a difference between the solution structure for both and the main-chain crystal structure of PA in this region. The data observed for PS *c*-551 are also present in PA *c*-551 spectra. First, chemical shifts for resonances in the loop region are highly homologous for both PA and PS. Second, d_{NN} NOE's for residues 35 and

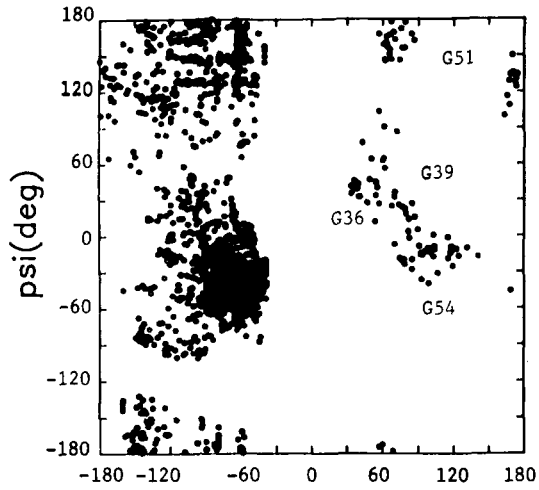

FIGURE 8: Ramachandran plot for the 24 SA structures.

36 and $d_{\alpha N}$ NOE's for residues 36 and 37 were not observed, while they should show very strong NOE's if there were a type I turn in solution (Billeter et al., 1982). By suitable choice of temperature and pH, clear 2D NMR spectral windows around these amides could be obtained, and we feel it is highly unlikely that the critical NOE's were missed because of overlap problems. In principle, there are cross-relaxation situations whereby an NOE is not observed between protons close in space, but in practice, we have observed NOE's in spectra of PA and PS *c*-551 for all other pairs of protons so close, on the basis of the crystal coordinates of PA *c*-551. Third, the main-chain dihedral angle of residue 35 is 26° in the crystal structure of PA *c*-551. This would predict a relatively strong scalar coupling from the amide proton to the α proton (θ = −34°, and a Karplus relation predicted J = 6.6 Hz). However, very small coupling constants were observed for both proteins. Unfortunately, these are consistent with the SA conformational alternatives discussed previously. Finally, a d_{NN} NOE was observed between residues 37 and 38 for both PA and PS *c*-551. In PA *c*-551, when NOE's were observed between any other two amide protons, the distances based upon the crystal coordinates were on the order of 3 Å or less between them. But in the 37–38 case, the crystal coordinates indicate d_{NN} is 4.6 Å, while the distance is 2.90 ± 0.52 Å for the 24 SA structures of PS *c*-551.

The crystallographic analysis had indicated this loop was a trouble spot. Especially significant is Figure 6 in Matsuura et al. (1982), the X-ray refinement report. The mean temperature factors for the main-chain atoms of residues 34–40 are among the highest in the crystal structure. This would represent large thermal motions and/or relative disorder in the crystal. The only residues with larger temperature factors

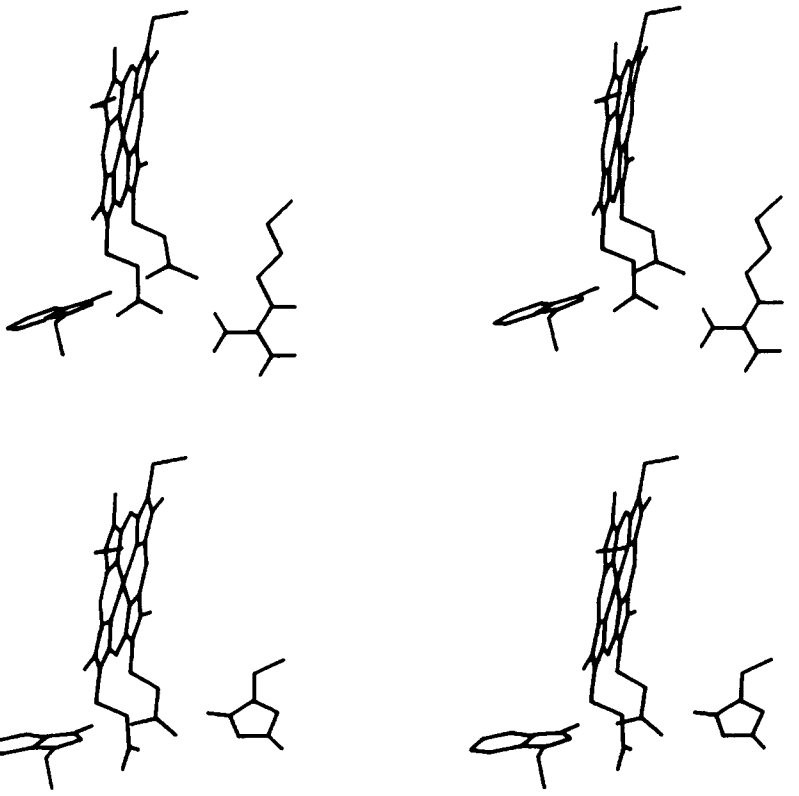

FIGURE 9: Hydrogen-bond differences involving the heme inner propionate and Arg 47 in PA *c*-551 (top) and His 47 in PS *c*-551 (bottom). Only the NH protons have been drawn in the figure.

FIGURE 10: Stereoview of the superposition of the side chains around Lys 33 from the 24 SA structures illustrating the hydrophobic packing. Lys 33 is at the bottom, Trp 56 is to the left and front, Val 55 is to the left and rear, Tyr 34 is to the rear, and Val 30 is to the top and right.

are 81 and 82 at the C-terminus. The loop at 36–40 is not at an intermolecular contact point in the crystal lattice. It could be that very high ionic strength (crystals were grown in 40–60% ammonium sulfate with 1 M NaCl) could cause a difference between solution and crystal. It is not likely that pH is important, because the crystallization pH was 5.6–5.7, similar to the value of 4.8 where most of the NMR data were collected. It is conceivable that the loop is quite flexible, with conformers represented by the NMR results, while crystallization froze out one alternative conformer.

Trp 56 and Gly 57. No side-chain substitutions occur from residues 51 to 64. However, the SA structures showed some differences for 56–60. The key change is the main-chain rotation of Gly 57 and Trp 56. The result is driven by rotational energy, because both the SA and the crystal conformations are consistent with the available NMR constraints. Trp 56 and Pro 58 have more favorable Ramachandran angles in the computed solution structure. The X-ray analysis again noted high temperature factors for residues 54 and 56.

Hydrogen Bonding of His 47. The heme is relatively buried in the polypeptide of *c*-551. Polar propionic acid substituents are stabilized by extensive hydrogen bonds. In the crystal structure of PA *c*-551, the inner propionate has one carboxyl oxygen hydrogen-bonded to Trp 56 Nϵ and the other to Arg 47 Nπ, and solution NMR data for PA *c*-551 are consistent with this geometry (Chau et al., 1990). In PS there is an interesting residue substitution to His 47. In the 24 SA structures for PS *c*-551, there is evidence for hydrogen bonding. The average N–H to propionate O distance for Trp 56 Nϵ is 2.38 Å and the average N–H–O angle is 135°. When electrostatics are included in the force field, these values improve to 1.86 Å and 158°, and with hydrogen-bonding terms, to 1.81 Å and 156°. For His 47, it is the Nπ proton that is an average distance of 2.24 Å from the other oxygen with an average angle of 120°. With electrostatics these values improve to 1.75 Å and 132°, and they remain the same when hydrogen-bonding terms are added. Figure 9 compares the hydrogen-bonding patterns in PA and PS. The extended length of the side chain of His 47 is not as long as for an arginine residue. It can form a hydrogen bond but must do so by interacting from a different direction. Arg 47 can be described as forming a hydrogen bond from the bottom of the heme crevice, while His 47 forms an analogous bond but from near the top corner. There are several NOE's that establish the orientation of the His 47 side chain about the β–γ bond as shown in Figure 9. These are NOE's from the C5H to the main-chain α and β protons and interresidue NOE's from C2H to the two methyl groups of Val 55, which are not shown in the figure but would be just beneath the carboxylate.

Our best current interpretation of 2D NMR cross-peak data indicates that the two NH protons of the imidazolium ring are in fast exchange with solvent (Cai & Timkovich,

1991). Figure 9 has been drawn showing only the NH protons on Arg 47, His 47, and Trp 56, and no information about the pK_a's of these groups or the propionates is intended. The protonation behavior of the ionizable groups in this network is complicated and will be presented in a later paper.

Lys 33. Both PS and PA *c*-551 contain eight lysine residues. Among these, Lys 33 in both proteins was a special residue in the sense that scalar couplings were very strong among its side-chain protons. It showed pronounced cross peaks in DQF-COSY spectra with large antiphase separations. Its spin system could be traced out in short spin lock time HOHAHA spectra. The multiple relay through-bond connectivities could be traced from α to ϵ in HOHAHA spectra with spin lock times as short as 20 ms, while times in excess of 50 ms were required for other lysines. Polylysine (Sigma Chemical Co., molecular weight range 1000–4000) was studied as a model compound. Polylysine does not have a fixed globular three-dimensional conformation, and presumably its side chains are freely rotating. HOHAHA spectra showed that the long-range connectivities from α to ϵ could only be made with spin lock times longer than 50 ms. Thus all lysines in PA and PS *c*-551 are like polylysine except for Lys 33.

Lys 33 is on the surface of the protein. As shown in Figure 10 for the 24 SA structures, the side chain was located in a hydrophobic groove on the protein surface created by the side chains of Val 30, Tyr 34, Trp 36, and Val 55 and constrained there by NOE's from these side chains to the Lys 33 side-chain protons. The terminal amine was not constrained and rotation about the δ–ϵ carbon–carbon single bond placed it 4.8 Å from the carbonyl oxygen of Val 55. When electrostatic terms were added to the refinement, this distance decreased to 3.39 Å by rotation about the single bond, and when hydrogen-bonding terms were added, it decreased to 3.13 Å. Association with the hydrophobic groove could hinder rotation about single bonds in Lys 33 and favor side-chain dihedral angles that lead to stronger coupling than in a purely rotationally averaged side chain.

ACKNOWLEDGMENT

We are extremely grateful to several individuals for helping us to obtain software while it was still under development and for their patience and advice with respect to questions of usage: for NMR4, Drs. P. A. Kollman, P. E. Wright, S. Harvey, and especially D. Case; for X-PLOR/dg, Dr. A. T. Brünger. Fully developed versions are now available as AMBER 4.0 from the UCSF group and as X-PLOR 3.0 from the Yale group.

REFERENCES

Almassy, R. J., & Dickerson, R. E. (1978) *Proc. Natl. Acad. Sci. U.S.A. 75*, 2674–2678.
Ambler, R. P. (1963a) *Biochem. J. 89*, 341–349.
Ambler, R. P. (1963b) *Biochem. J. 89*, 349–378.
Ambler, R. P. (1982) in *From Cyclotrons to Cytochromes* (Kaplan, N. O., & Robinson, A., Eds.) pp 263–280, Academic Press, New York.
Ambler, R. P., & Wynn, M. (1973) *Biochem. J. 131*, 485–498.
Berendsen, H. J. C., Postma, J. P. M., van Gunsteren, W. F., DiNola, A., & Haak, J. R. (1984) *J. Chem. Phys. 81*, 3684–3690.
Billeter, M., Braun, W., & Wüthrich, K. (1982) *J. Mol. Biol. 155*, 321–346.
Brooks, B. R., Bruccoleri, R. E., Olafson, B. D., States, D. J., Swaminathan, S., & Karplus, M. (1983) *J. Comput. Chem. 4*, 187–217.
Brünger, A. T., & Karplus, M. (1991) *Acc. Chem. Res. 24*, 54–61.
Cai, M. (1991) Ph.D. Thesis, University of Alabama, Tuscaloosa, AL.
Cai, M., & Timkovich, R. (1991) *Biochem. Biophys. Res. Commun. 178*, 309–314.
Chau, M. H., Cai, M. L., & Timkovich, R. (1990) *Biochemistry 29*, 5076–5087.
Clore, G. M., Gronenborn, A. M., Nilges, M., & Ryan, C. A. (1987) *Biochemistry 26*, 8012–8023.
Crawford, J. L., Lipscomb, W. N., & Schellman, C. G. (1973) *Proc. Natl. Acad. Sci. U.S.A. 70*, 538–542.
Detlefsen, D. J., Thanabal, V., Pecoraro, V. L., & Wagner, G. (1990) *Biochemistry 29*, 9377–9386.
Detlefsen, D. J., Thanabal, V., Pecoraro, V. L., & Wagner, G. (1991) *Biochemistry 30*, 9040–9046.
Dickerson, R. E., & Timkovich, R. (1975) in *The Enzymes* (Boyer, P. D., Ed.) pp 397–547, Academic Press, New York.
Dickerson, R. E., Timkovich, R., & Almassy, R. J. (1976) *J. Mol. Biol. 100*, 473–491.
Driscoll, P. C., Gronenborn, A. M., Beress, L., & Clore, G. M. (1989) *Biochemistry 28*, 2188–2198.
Dyson, H. J., Gippert, G. P., Case, D. A., Holmgren, A., & Wright, P. E. (1990) *Biochemistry 29*, 4129–4136.
Gao, Y., Lee, A. D. J., Williams, R. J. P., & Williams, G. (1989) *Eur. J. Biochem. 182*, 57–65.
Gippert, G. P., Yip, P. F., Wright, P. E., & Case, D. A. (1990) *Biochem. Pharmacol. 40*, 15–22.
Kamen, M. D., & Horio, T. (1970) *Annu. Rev. Biochem. 39*, 673–701.
Kuszewski, J., Nilges, M., & Brünger, A. T. (1992) *J. Biomol. NMR 2*, 33–56.
Levitt, M. (1982) *Annu. Rev. Biophys. Bioeng. 11*, 251–271.
Matsuura, Y., Takano, T., & Dickerson, R. E. (1982) *J. Mol. Biol. 156*, 389–409.
Meyer, T. E., & Kamen, M. D. (1982) *Adv. Protein Chem. 35*, 105–212.
Nilges, M., Clore, G. M., & Gronenborn, A. M. (1988) *FEBS Lett. 229*, 317–324.
Parr, S. R., Barber, D., Greenwood, C., Phillips, B. W., & Melling, J. (1976) *Biochem. J. 157*, 423–430.
Robinson, M. K., Martinkus, K. J., Kennelly, P. J., & Timkovich, R. (1979) *Biochemistry 18*, 3921–3926.
Timkovich, R. (1990) *Biochemistry 29*, 7773–7780.
Timkovich, R. (1991) *Inorg. Chem. 30*, 37–42.
Wagner, G., Braun, W., Havel, T. F., Schaumman, T., Go, N., & Wüthrich, K. (1987) *J. Mol. Biol. 196*, 611–639.
Weiner, P. K., & Kollman, P. A. (1981) *J. Comput. Chem. 2*, 287–303.
Weiner, S. J., Kollman, P. A., Nguyen, D. T., & Case, D. A. (1986) *J. Comput. Chem. 7*, 230–252.
Williamson, M. P., Havel, T. F., & Wüthrich, K. (1985) *J. Mol. Biol. 182*, 295–312.
Wüthrich, K., Billeter, M., & Braun, W. (1983) *J. Mol. Biol. 169*, 949–961.
Zuiderweg, E. R. P., Boelens, R., & Kaptein, R. (1985) *Biopolymers 24*, 601–611.

Registry No. His, 71-00-1; cytochrome *c*-551, 9048-77-5.